Physics Letters B 751 (2015) 12–18

Contents lists available at ScienceDirect

Physics Letters B

www.elsevier.com/locate/physletb

First observation of long-lived $\pi^+\pi^-$ atoms

DIRAC Collaboration

B. Adeva [a], L. Afanasyev [b], A. Anania [c], S. Aogaki [d], A. Benelli [e], V. Brekhovskikh [f], T. Cechak [e], M. Chiba [g], P. Chliapnikov [f], P. Doskarova [e], D. Drijard [h], A. Dudarev [b], M. Duma [d], D. Dumitriu [d], D. Fluerasu [d], A. Gorin [f], O. Gorchakov [b], K. Gritsay [b], C. Guaraldo [i], M. Gugiu [d], M. Hansroul [h], Z. Hons [j], S. Horikawa [k], Y. Iwashita [l], V. Karpukhin [b], J. Kluson [e], M. Kobayashi [m], V. Kruglov [b], L. Kruglova [b], A. Kulikov [b], E. Kulish [b], A. Kuptsov [b], A. Lamberto [c], A. Lanaro [n], R. Lednicky [o], C. Mariñas [a], J. Martincik [e], L. Nemenov [b,h], M. Nikitin [b], K. Okada [p], V. Olchevskii [b], V. Ovsiannikov [q], M. Pentia [d], A. Penzo [r], M. Plo [a], P. Prusa [e], G. Rappazzo [c], A. Romero Vidal [a], A. Ryazantsev [f], V. Rykalin [f], J. Saborido [a], J. Schacher [s,*], A. Sidorov [f], J. Smolik [e], F. Takeutchi [p], L. Tauscher [t], T. Trojek [e], S. Trusov [u], T. Urban [e], T. Vrba [e], V. Yazkov [u], Y. Yoshimura [m], M. Zhabitsky [b], P. Zrelov [b]

[a] *Santiago de Compostela University, Spain*
[b] *JINR, Dubna, Russia*
[c] *INFN, Sezione di Trieste and Messina University, Messina, Italy*
[d] *IFIN-HH, National Institute for Physics and Nuclear Engineering, Bucharest, Romania*
[e] *Czech Technical University in Prague, Czech Republic*
[f] *IHEP, Protvino, Russia*
[g] *Tokyo Metropolitan University, Japan*
[h] *CERN, Geneva, Switzerland*
[i] *INFN, Laboratori Nazionali di Frascati, Frascati, Italy*
[j] *Nuclear Physics Institute ASCR, Rez, Czech Republic*
[k] *Zurich University, Switzerland*
[l] *Kyoto University, Kyoto, Japan*
[m] *KEK, Tsukuba, Japan*
[n] *University of Wisconsin, Madison, USA*
[o] *Institute of Physics ASCR, Prague, Czech Republic*
[p] *Kyoto Sangyo University, Kyoto, Japan*
[q] *Voronezh State University, Russia*
[r] *INFN, Sezione di Trieste, Trieste, Italy*
[s] *Albert Einstein Center for Fundamental Physics, Laboratory of High Energy Physics, Bern, Switzerland*
[t] *Basel University, Switzerland*
[u] *Skobeltsin Institute for Nuclear Physics of Moscow State University, Moscow, Russia*

ARTICLE INFO

Article history:
Received 23 July 2015
Received in revised form 7 September 2015
Accepted 23 September 2015
Available online 9 October 2015
Editor: M. Doser

ABSTRACT

After observing and investigating the double-exotic (a double-exotic atom is a bound system, in which both oppositely charged components are unstable particles like $\mu, \pi, K, \ldots$) $\pi^+\pi^-$ atom with the ground state lifetime τ of about 3×10^{-15} s, the upgraded DIRAC experiment at the CERN PS accelerator observes for the first time long-lived states of the same atom with lifetimes of about 10^{-11} s and more. The number of characteristic pion pairs resulting from the breakup (ionisation) of long-lived $\pi^+\pi^-$ atoms amounts to 436 ± 61, corresponding to a signal-to-error ratio of better than 7 standard deviations. This

* Corresponding author.
E-mail address: schacher@lhep.unibe.ch (J. Schacher).

http://dx.doi.org/10.1016/j.physletb.2015.09.060

observation opens a new possibility to measure energy differences between p and s atomic states and so to determine $\pi\pi$ scattering lengths.

1. Introduction

The experimental program of the DIRAC Collaboration comprises the observation and detailed analysis of dimesonic atoms, which are produced by protons interacting with target nuclei [1]. First, DIRAC has investigated $\pi^+\pi^-$ atoms (pionium, $A_{2\pi}$) and measured their lifetime, $\tau = (3.15^{+0.28}_{-0.26})$ fs, in the ground state and hence a combination of $\pi\pi$ scattering lengths [2]. Second, evidence for the production of dimesonic atoms with strangeness, i.e. πK atoms, has been found [3]. The data analysis has yielded a first measurement of the πK atom lifetime and πK scattering lengths [4]. Third, a search for long-lived $\pi\pi$ atom states has been performed. DIRAC plans to study the *Lamb shift* in $\pi\pi$ atoms and then to extract another $\pi\pi$ scattering length combination. A similar measurement for long-lived πK atoms can be performed providing additional information about πK scattering lengths. In this paper DIRAC presents the first observation of more than 400 long-lived $\pi^+\pi^-$ atoms.

The decay probability of $\pi^+\pi^-$ atoms is dominated by the annihilation process

$$\pi^+ + \pi^- \to \pi^0 + \pi^0 \tag{1}$$

(branching ratio $\sim 99.6\%$) and depends on the difference between the S-wave $\pi\pi$ scattering lengths with isospins zero (a_0) and two (a_2) [5–8]:

$$\frac{1}{\tau} \approx W_{\pi^0\pi^0} = R\,|a_0 - a_2|^2 \quad \text{with} \quad R \propto |\psi_{nl}(0)|^2\,. \tag{2}$$

The expression $\psi_{nl}(0)$ is the pure Coulomb atomic wave function at the origin with principal quantum number n and angular momentum quantum number l. The most accurate ratio R has been derived with a precision of 1.2% in [9].

In order to get values of a_0 and a_2 separately from $\pi^+\pi^-$ atom data, one may exploit the fact that the energy splitting between the levels ns and np, $\Delta E^{ns-np} = E_{ns} - E_{np}$, depends on another combination of the scattering lengths: $2a_0 + a_2$ [10]. The influence of strong and electromagnetic interactions on the $A_{2\pi}$ energy structure has been studied in [10–14] and a detailed analysis performed in [15]. The energy shift for the levels with the principal quantum number n and orbital quantum number l is composed of three contributions: $\Delta E_{nl} = \Delta E^{\rm em}_{nl} + \Delta E^{\rm vac}_{nl} + \Delta E^{\rm str}_{nl}$. The term $\Delta E^{\rm em}_{nl}$ includes relativistic insertions, finite-size effect, self-energy corrections due to transverse photons and transverse photon exchange. Contributions from vacuum polarization are covered by $\Delta E^{\rm vac}_{nl}$. The last term $\Delta E^{\rm str}_{nl}$ takes into account effects from strong interaction and is related to the $\pi\pi$ scattering lengths according to: $\Delta E^{\rm str}_{n0} = A_n(2a_0 + a_2)$. The theoretical value for the $2s-2p$ energy splitting amounts to $\Delta E^{2s-2p} = (-0.59 \pm 0.01)$ eV, whereas the splitting ΔE^{ns-np} for higher principal quantum numbers n decreases [15]. By measuring the value of ΔE^{ns-np}, one can determine the numerical value of $\Delta E^{\rm str}_{n0}$, as all other terms in ΔE_{nl} have been calculated with high precision: the strong interaction effects contribute up to 80% of the full energy shift. This fact provides a high sensitivity of a ΔE^{2s-2p} measurement to the value of the term $2a_0 + a_2$. Thus, a measurement of the energy shift ΔE^{ns-np} allows to obtain a value for the new combination of scattering lengths $2a_0 + a_2$.

A method to measure ΔE^{ns-np} has been proposed in [1]. By investigating the influence of an applied electric or magnetic field on the decay probability of long-lived $\pi^+\pi^-$ atom states $A^L_{2\pi}$ ($l \geq 1$), it is possible to extract an experimental value for ΔE^{ns-np} [19,20].

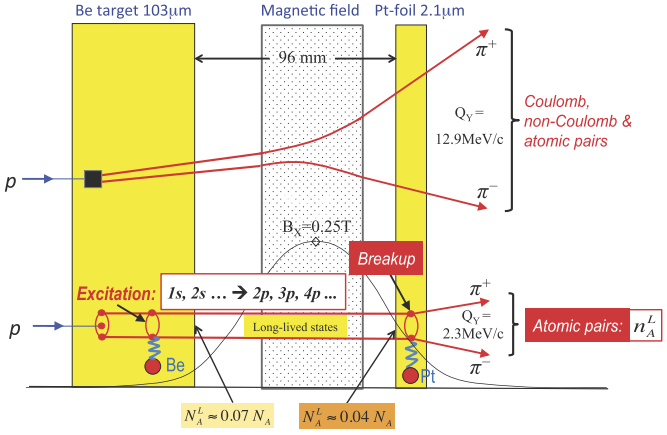

Fig. 1. Method to observe long-lived $A^L_{2\pi}$ by means of a breakup foil (Pt).

In inclusive processes $A_{2\pi}$ atoms are produced in s-states distributed over the principal quantum number n according to n^{-3}. When moving inside the target, relativistic $A_{2\pi}$ interact with the electric field of target atoms, and some of them (N^L_A) leave the target with an orbital quantum number $l > 0$. The main primary excitation process is the transition $ns \to n'p$. Then, for excited states with $l \geq 1$, the decays of $A^L_{2\pi}$ into two π^0, $\pi^0 + \gamma$ and two γ are suppressed in accordance with (2) because of $|\psi_{nl}(0)|^2 = 0$ [19]. Therefore, the decay mechanism of such excited states is the radiative deexcitation to an ns state, annihilating subsequently with the lifetime $\tau \cdot n^3$ into two π^0. Thus, the $A^L_{2\pi}$ decay probability is given by the shortest radiative lifetime, the $2p$ lifetime $\tau_{2p} = 1.17 \cdot 10^{-11}$ s. For an average $A_{2\pi}$ momentum of 4.5 GeV/c ($\gamma \simeq 16$), the decay lengths are 5.7 cm ($2p$), 19 cm ($3p$) and 43 cm ($4p$). Using a $\sim$100 μm thick Be target and inserting a $\sim$2 μm thick Pt foil downstream of this target [21], a large fraction of the long-lived atoms $A^L_{2\pi}$, generated in Be, reaches the Pt foil and breaks up, thus providing an extra number n^L_A of atomic pairs (see Fig. 1).

In order to be able to claim "observation of long-lived $A^L_{2\pi}$" – the goal of this investigation – the DIRAC setup has been modified in 2012 as described in the following section.

The most accurate theoretical predictions for the S-wave $\pi\pi$ scattering lengths have been achieved in [16] (in units $M^{-1}_{\pi^+}$):

$$a_0 = 0.220 \pm 0.005\,, \quad a_2 = -0.0444 \pm 0.0010\,,$$
$$a_0 - a_2 = 0.265 \pm 0.004\,. \tag{3}$$

The best experimental results with a precision of around 4% have been obtained from studying the decays $K^\pm \to \pi^+\pi^- e^\pm \nu$ [17] and $K^\pm \to \pi^\pm\pi^0\pi^0$ [18] as well as from measuring the $\pi^+\pi^-$ atom lifetime [2]: $|a_0 - a_2| = \left(0.2533^{+0.0112}_{-0.0107}\right)$. In the case of K decays, additional theoretical information can improve the experimental scattering length values [17,18].

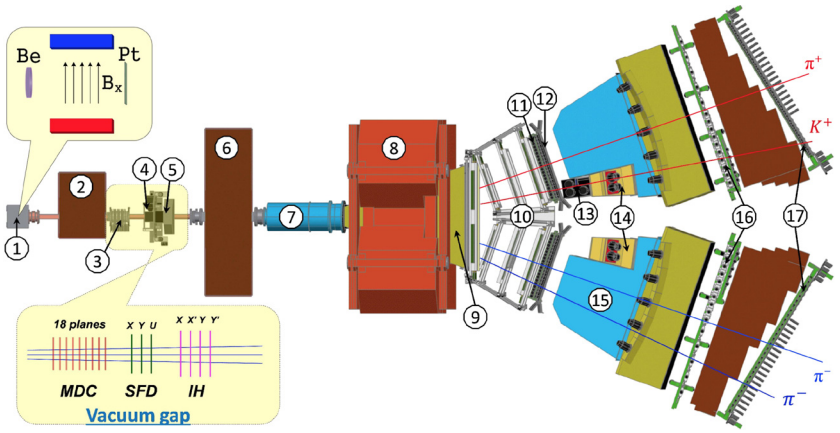

Fig. 2. General view of the DIRAC setup: 1 – target station with insertion, showing the Be target, magnetic field and Pt breakup foil; 2 – first shielding; 3 – microdrift chambers (MDC); 4 – scintillating fiber detector (SFD); 5 – ionisation hodoscope (IH); 6 – second shielding; 7 – vacuum tube; 8 – spectrometer magnet; 9 – vacuum chamber; 10 – drift chambers (DC); 11 – vertical hodoscope (VH); 12 – horizontal hodoscope (HH); 13 – aerogel Cherenkov; 14 – heavy gas Cherenkov; 15 – nitrogen Cherenkov; 16 – preshower (PSh); 17 – muon detector. (The plotted symmetric and asymmetric events are a $\pi\pi$ and πK pair, respectively.)

2. Setup for detection of long-lived $\pi^+\pi^-$ atoms

The DIRAC setup [22] is sketched in Fig. 2. A high-resolution magnetic spectrometer ($\Delta p/p \simeq 3 \cdot 10^{-3}$) is used to split oppositely charged meson pairs ($\pi^+\pi^-$ and $\pi^\mp K^\pm$) and to measure their relative c.m. momentum (Q) with good precision in order to extract a dimeson atom signal [2,4]. The 24 GeV/c CERN PS proton beam interacting with the target produces additionally free (unbound) "Coulomb pairs" from short-lived resonances, "non-Coulomb pairs" from long-lived sources and accidental coincidences (different proton–nucleus interactions). Therefore, the atom signal suffers from a $\pi^+\pi^-$ continuum background causing the main signal uncertainty.

In the search for long-lived $A_{2\pi}^L$, the primary proton beam hits a 103 μm thick 99.98% pure Be target, providing the needed $A_{2\pi}^L$ yield at an acceptable proton beam intensity [21]. The target radiation thickness amounts to $3.0 \cdot 10^{-4}$ X_0 (radiation length) and the nuclear interaction probability to $\varepsilon_{nuc} = 2.5 \cdot 10^{-4}$. The secondary channel with the whole setup is vertically inclined relative to the proton beam by 5.7° upward. By means of a rectangular beam collimator inside of the second steel shielding wall (Fig. 2, item 6), secondary particles are confined to ±1° in the horizontal (X) and vertical (Y) planes and thus to the solid angle $\Omega = 1.2 \cdot 10^{-3}$ sr. Downstream of the Be target, a 2.1 μm thick Pt foil ($6.9 \cdot 10^{-4}$ X_0, $\varepsilon_{nuc} = 0.23 \cdot 10^{-4}$) for $A_{2\pi}^L$ breakup has been placed at a distance of 96 mm. The foil is installed at 7.5 mm above the primary proton beam to avoid interaction of the beam halo with Pt (Fig. 1). The upper limit of the beam size in the vertical direction is $\sigma_y = 1.75$ mm [30]. The beam position in the vertical plane has been permanently monitored during the run by checking SFD and IH counting rates and by reconstructing the beam position with track information (Fig. 3). Between target and breakup foil, a permanent magnet [23] has been introduced to suppress significantly background $\pi^+\pi^-$ pairs, generated in Be, in the low Q region, where the atomic pairs from $A_{2\pi}^L$ breakup are expected (Fig. 1). The retractable magnet with a pole distance of 60 mm consists of a Samarium–Cobalt alloy (Sm_2Co_{17}) and has a maximum horizontal field strength of 0.25 T (see insertion in Fig. 2). The bending power of 0.02 Tm is relatively homogeneous in the secondary beam region, with a precision of better than ±2%.

In order to measure the shift of the vertical component Q_Y, which is enlarged by the horizontal magnetic field, e^+e^- Dalitz pairs generated in the Be target as well as e^+e^- pairs produced in the Pt foil by photons have been investigated. The experimental Q_Y distribution (Fig. 4a) shows a first peak around originating

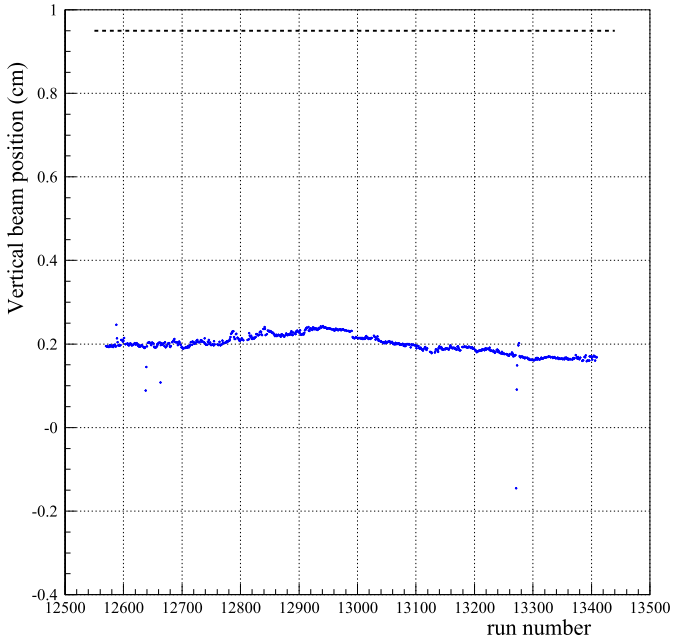

Fig. 3. Vertical coordinate of the beam position (dots) on the Beryllium target, reconstructed with track information for all data runs. The low edge of the Platinum foil is shown as dashed line.

from pairs produced far downstream of the magnet and a second peak from Dalitz pairs at $Q_Y = 12.9$ MeV/c. After subtracting the left part of the central peak ($Q_Y \approx 0$) from the right part (mirrored subtraction), a peak at $Q_Y = 2.3$ MeV/c appears from e^+e^- pairs produced in Pt and crossing only the fringing magnetic field [24] (Fig. 4b). The experimental peak positions as well as the shapes coincide with simulation, which has been obtained by using the magnetic field map with a precision of better than 1% [25]. Each oppositely charged particle pair, generated in the Be target and hence crossing the magnetic field region, obtains an additional ΔQ_Y of 12.9 MeV/c, whereas a pair produced in the Pt foil gets a smaller ΔQ_Y, caused by the fringing field, of only 2.3 MeV/c. This difference in the Q_Y shift for pairs from Be and Pt allows to suppress significantly the background level for observing atomic pairs from long-lived $A_{2\pi}^L$.

The peak position for Dalitz pairs at $Q_Y = 12.9$ MeV/c has been used to control the magnetic field stability during the 6 month

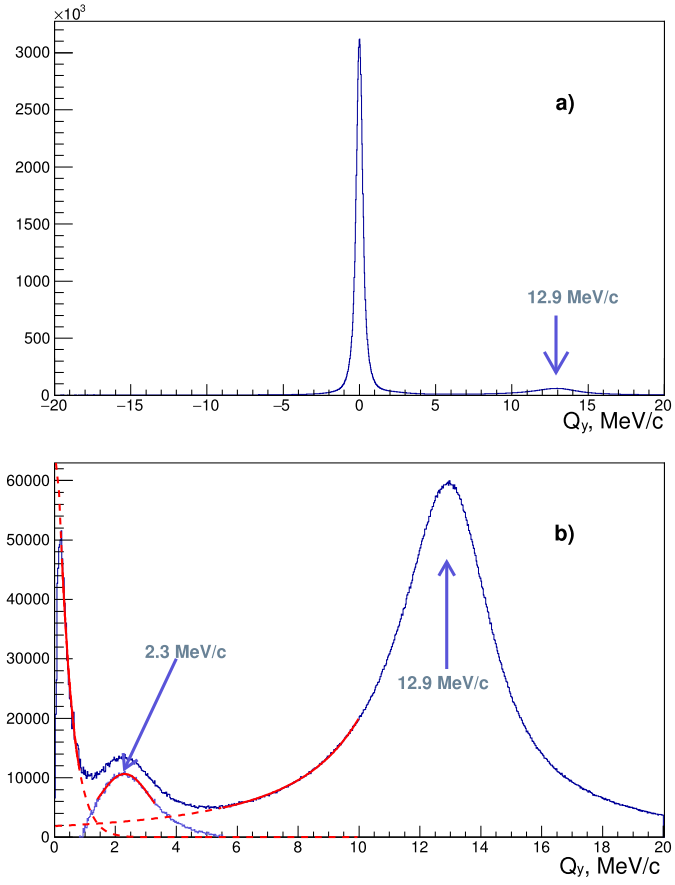

Fig. 4. a) Experimental distribution of e^+e^- pairs on Q_Y. b) Same distribution after mirror subtraction.

data taking in 2012: the field strength of the Sm_2Co_{17} magnet[1] has been stable within a relative precision of better than $5 \cdot 10^{-4}$ [25].

With a spill duration of 450 ms the beam intensity has been $(28–30) \cdot 10^{10}$ protons/spill.

3. Event reconstruction

The event reconstruction has been performed by means of the DIRAC $\pi\pi$ analysis software already used for the analysis of the 2001–2003 data [2]. Only events with one or two so-called DC tracks – tracks reconstructed only with DC hits – in each arm are processed according to the following criteria:

1) One or two hadron tracks are identified in the DC of both arms with corresponding hits in VH, HH and PSh, but no signal in ChN and Mu detectors (Fig. 2). In each arm the earliest track, which initiates the readout procedure, is selected for further analysis.

2) The DC tracks are extrapolated backward to the incident proton beam position on the target using the inverse transfer function of the DIRAC dipole magnet. This procedure provides a first approximation of the particle momenta and the corresponding intersection points in MDC, SFD and IH.

3) SFD hits are searched for in the coordinate region defined by the position accuracy: a square of size ± 1 cm, that corresponds to 5σ for high momentum and to 3σ for low momentum particles.

[1] Under the same radiation condition the field strength of a permanent Nd–Fe–B magnet has been decreased by more than 50% during the 2011 run [26].

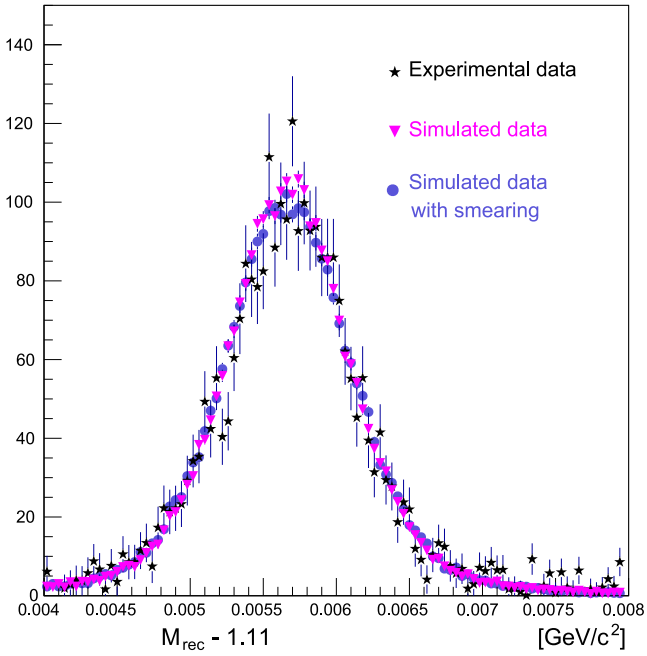

Fig. 5. Invariant π^-p mass distribution in the Λ region.

The two tracks should not use a common SFD hit in case of more than one hit in the proper region. If the number of hits around the two tracks is ≤ 4 in each SFD plane and ≤ 9 in all 3 SFD planes, the event is kept. These cuts reduce the data sample by 1/3, which is then called "low and medium background events". A further adjustment is applied in order to find the best two-track combination: The momenta of the positively and negatively charged particle are modified to match the DC track X-coordinates and the SFD hits in the X- or U-plane. In the final analysis, the combination with the best χ^2 in the SFD planes and vertex in the target is selected.

The setup has been aligned using properties of Λ ($\bar{\Lambda}$) decays [27]. The decay particles are reconstructed and the corresponding invariant mass determined. The introduced permanent magnet (Fig. 2) implies a bias in the Y-components of the charged decay particle momenta. The bias amplitude depends on the decay vertex position inside the magnet. One observes a shift of the mass peak position and an increase in the width of the mass distribution. Therefore, data with magnetic field only allows to check the equality of the Λ and $\bar{\Lambda}$ masses. In order to check the Λ mass value, a special data set without magnet has been collected (about 7% of the total data set). The distribution of reconstructed Λ masses is presented in Fig. 5. The experimental value $M_\Lambda = 1.11568 \pm 0.00001$ GeV/c^2 is in good agreement with the PDG value $M_\Lambda^{\rm PDG} = 1.115683 \pm 0.000006$ GeV/c^2. Investigations of data collected in 2008–2010 [27] have shown that the width of the simulated Λ distribution is narrower than the experimental one, due to underestimation of the uncertainty in particle momentum reconstruction. To improve simulation, a Gaussian smearing of reconstructed momenta has been introduced: $p^{\rm smeared} = p(1 + C_f \cdot N(0,1))$. This smearing of simulated momenta with $C_f = (7 \pm 4) \cdot 10^{-4}$ leads to a reconstructed Λ width consistent with experimental data (Fig. 5). The momentum resolution has been evaluated by investigating simulated events. For each track the reconstructed momentum between 1.5 and 8 GeV/c is compared with the generated one. The relative precision lies within $2.8 \cdot 10^{-3}$ to $4.4 \cdot 10^{-3}$. The resolutions in the components of the relative pair momentum Q, without taking into account

Table 1
Relative populations ε_n(Be) and ε_n(Pt) as a function of n (summed over l and m).

n	2	3	4	5	≥ 2
ε_n(Be) $\times 10^2$	$2.48 \pm O(10^{-3})$	1.54 ± 0.01	0.86 ± 0.03	0.56 ± 0.06	6.8 ± 0.6
ε_n(Pt) $\times 10^2$	$0.52 \pm O(10^{-4})$	$1.10 \pm O(10^{-3})$	0.78 ± 0.03	0.54 ± 0.06	4.3 ± 0.6

target multiple scattering, are $\sigma(Q_X) = \sigma(Q_Y) = 0.44$ MeV/c and $\sigma(Q_L) = 0.50$ MeV/c.

4. Simulation

A generator, called DIPGEN [28], is used to simulate $\pi^+\pi^-$ pairs (atomic pairs, Coulomb and non-Coulomb pairs), which are generated in the Be target and Pt foil. For long-lived atoms the following quantities are evaluated:

1. Ratio ε_{nlm}(Be) between number $N_A^{L,\mathrm{Be}}$ of long-lived atoms, which exit the Be target, and total number N_A of produced atoms as a function of atom quantum numbers n, l, m: $N_A^{L,\mathrm{Be}}(n,l,m) = \varepsilon_{nlm}(\mathrm{Be}) \times N_A$;
2. Atom decay probabilities in the space between Be and Pt as a function of n, l and atom momentum [29];
3. Ratio ε_{nlm}(Pt) between number $N_A^{L,\mathrm{Pt}}$ of long-lived atoms at the Pt foil entry and total number of produced atoms: $N_A^{L,\mathrm{Pt}}(n,l,m) = \varepsilon_{nlm}(\mathrm{Pt}) \times N_A$;
4. Breakup probability W_{br} in Pt as a function of n, l and m.

In Table 1, the relative population of long-lived atom states as a function of n is given at the exit of the Be target and at the entry of the Pt foil taking into account their decay in-between.

The calculated number of long-lived atoms at the exit of the Be target is $N_A^{L,\mathrm{Be}} = (6.8 \pm 0.6) \cdot 10^{-2} \times N_A$. After passing the gap of 96 mm, (4.3 ± 0.6)% of the produced atoms enter the Pt foil. Their breakup probability in Pt varies in a wide range depending on the atom $|nlm\rangle$ state and momentum at the Pt foil entry: e.g. for an input 2p state with 4.5 GeV/c, it is about 0.7, while for a 5p state the breakup probability exceeds 0.95. As a result, the number of atomic pairs generated in Pt is $n_A^{L,\mathrm{calc}} = (4.0 \pm 0.7) \cdot 10^{-2} \times N_A$, which corresponds to an averaged breakup probability of $W_{\mathrm{br}} = 0.92$. The magnetic field between Be and Pt has not been considered. Its influence is a decrease of the number of atoms at the Pt foil entry [1,19] and will be studied in future. The atomic (Pt), Coulomb (Be) and non-Coulomb (Be) pair distributions of relative momentum projections q_x, q_y, q_L (initial, i.e. not smeared) at the breakup point as well as after multiple scattering have been simulated. In the next step, all pairs generated by DIPGEN are transferred to the GEANT-DIRAC (setup simulator) and ARIANE (reconstruction tool) programs. The distributions of the reconstructed values Q_L and Q_T of pairs from $A_{2\pi}^L$ breakup in Pt as well as of Coulomb and non-Coulomb pairs, generated in Be, are obtained. The majority of the atomic pairs from the breakup in Pt has a Q_T and Q_L of less than 1.5 MeV/c (Figs. 6 and 7). Moving in the fringing magnetic field, each atomic pair receives an additional $\Delta Q_Y = 2.3$ MeV/c. To get the initial value of Q_Y for atomic pairs from Pt, the reconstructed value must be reduced by this amount, leading to the initial value of the transverse momentum $Q_T = \sqrt{Q_X^2 + (Q_Y - 2.3\,\mathrm{MeV/c})^2}$.

5. Data analysis and results

The experimental distributions of $\pi^+\pi^-$ pairs as a function of relative momentum Q components have been fitted with simulated distributions of atomic pairs (n_A^L) from Pt, Coulomb (N_C) and non-Coulomb pairs (N_{nC}) from Be. The three corresponding numbers are free parameters in the fit.

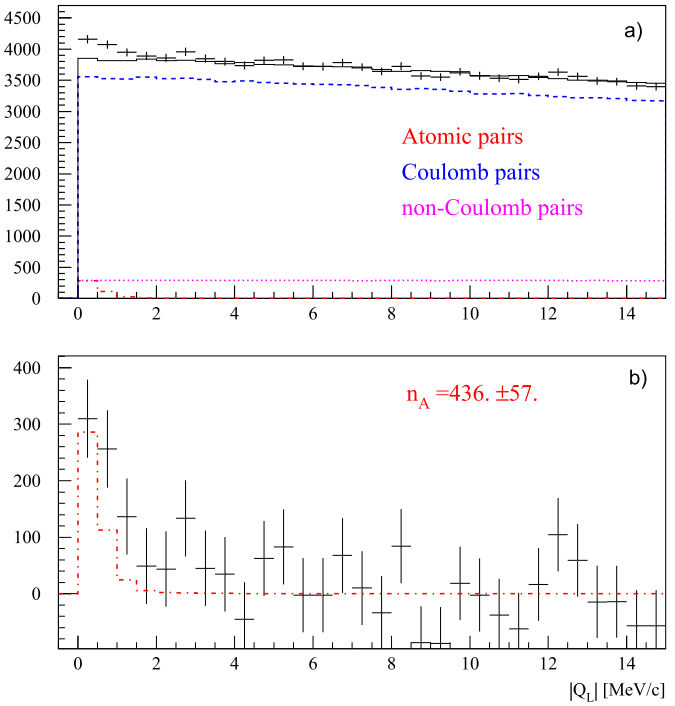

Fig. 6. $|Q_L|$ distribution of $\pi^+\pi^-$ pairs for $Q_T < 2.0$ MeV/c. The plot a) shows the experimental distribution (points with statistical error) and the simulated background (solid line). The plot b) shows the experimental distribution after background subtraction (points with statistical error) and the simulated distribution of atomic pairs (dotted-dashed line). The fit procedure has been applied to the 2-dimensional $(|Q_L|, Q_T)$ distribution.

In the 2-dimensional $(|Q_L|, Q_T)$ analysis, the experimental data have been analysed using simulated 2-dimensional distributions. For $|Q_L| < 15$ MeV/c and $Q_T < 2$ MeV/c, the $|Q_L|$ projection of the experimental 2-dimensional distribution as well as of the three types of simulated $\pi^+\pi^-$ pairs are shown in Fig. 6a. One observes an excess of events – above the sum of Coulomb and non-Coulomb pairs – in the low Q_L region, where atomic pairs are expected. After subtracting background, there is a statistically significant signal of $n_A^L = 436 \pm 57$ (Fig. 6b). The signal shape is compared with the simulated distribution of atomic pairs resulting from the long-lived atom breakup in the Pt foil. The description is acceptable, taking into account large statistical uncertainties induced by subtracting two large numbers in the bins of the signal distribution. The atomic pair selection efficiency for different cuts on Q_T is known from simulation. Using this efficiency the total number of atomic pairs generated in Pt is $n_A^{L,\mathrm{tot}} = 488 \pm 64$. Fig. 7a presents the Q_T projection of the same 2-dimensional distributions for $|Q_L| < 2$ MeV/c and $Q_T < 4$ MeV/c with the same free fit parameters. After background subtraction in the low Q region, one observes again a statistically significant signal with a shape described by the simulated Q_T distribution of atomic pairs from long-lived atom breakup in Pt (Fig. 7b). The number of atomic pairs in the region $Q_T < 4$ MeV/c is $n_A^L = 429 \pm 56$.

In the 1-dimensional analysis, the $|Q_L|$ distribution is fitted using different cuts $Q_T < 0.5$, 1.0, 1.5, 2.0 MeV/c to study the stability of the atomic pair number for different background levels. The

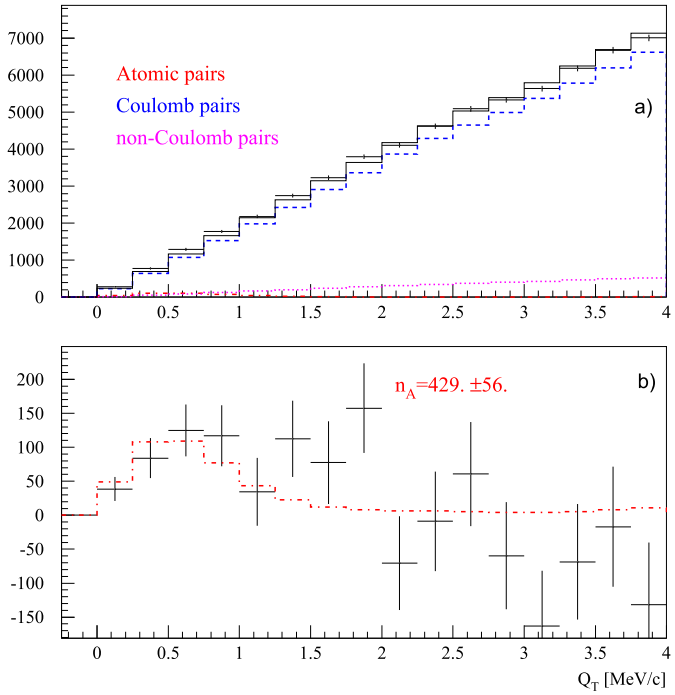

Fig. 7. Q_T distribution of $\pi^+\pi^-$ pairs for $|Q_L| < 2$ MeV/c. The plot a) shows the experimental distribution (points with statistical error) and the simulated background (solid line). The plot b) shows the experimental distribution after background subtraction (points with statistical error) and the simulated distribution of atomic pairs (dotted-dashed line). The fit procedure has been applied to the 2-dimensional $(|Q_L|, Q_T)$ distribution.

Table 2
Analysis of data collected in 2012 for different fitting procedures. The detected numbers n_A^L of atomic pairs and the corresponding total numbers $n_A^{L,\mathrm{tot}}$ (via selection efficiency) are presented together with the background contribution (Coulomb, non-Coulomb and accidental pairs) and the fit quality χ^2/n (n = degrees of freedom). Errors are only statistical.

Q_T cut (MeV/c)	n_A^L	$n_A^{L,\mathrm{tot}}$	Background	χ^2/n
2-dimensional fit over Q_L, Q_T				
2.0	436 ± 57	488 ± 64	16 790	138/140
1-dimensional fit over Q_L				
0.5	152 ± 29	467 ± 88	971	29/27
1.0	349 ± 53	489 ± 75	3692	19/27
1.5	386 ± 78	454 ± 91	9302	22/27
2.0	442 ± 105	495 ± 117	16 774	22/27

detected numbers n_A^L of atomic pairs and the corresponding total numbers are shown in Table 2. The background for $Q_T < 2$ MeV/c is 17 times higher than for $Q_T < 0.5$ MeV/c. Nevertheless, the values in the 1- and 2-dimensional analyses coincide within statistics. This confirms the signal stability for different Q_T cuts, i.e. for different background levels.

The measurement of the atomic pair number n_A^L is affected by the description accuracy of the simulated distributions for Coulomb, non-Coulomb and atomic pairs. If the shapes of the simulated distributions differ from the experimental ones, then the fit parameter values might be biased. In the long-lived atom search, the shapes of Coulomb and non-Coulomb pairs from Be are similar in phase-space (Figs. 6 and 7). Therefore, a systematic error might only arise from an incorrect description of the atomic pair distribution, due to the uncertainty in the Q_L and Q_T resolution [30].

There are two main sources of systematic errors in the number n_A^L of atomic pairs: 1) The Λ width correction accuracy (Section 3) leads to a systematic error of $\sigma_\Lambda^{\mathrm{syst}} = 4.4$. 2) The accuracy of the measured Pt foil thickness dominates the uncertainty in Q_T resolution, causing a systematic error of $\sigma_{\mathrm{Pt}}^{\mathrm{syst}} = 22$ in the 2-dimensional analysis. In the 1-dimensional $|Q_L|$ analysis, this error is nearly 0.

Another problem might arise from a hypothetical admixture of $\pi^+\pi^-$ Coulomb pairs generated by beam halo protons interacting with the Pt foil. A peak induced by Coulomb final state interaction would be at the same place as atomic pairs from breakup of long-lived atoms $A_{2\pi}^L$. The beam halo level and interaction rate with Pt have been investigated [31] with the result that the flux of Coulomb pairs, generated in Pt, is practically negligible compared to the number n_A^L of atomic pairs from $A_{2\pi}^L$ breakup under working condition. To minimize any wrong interpretation, data have been additionally analysed under the assumption that they originate from Coulomb pairs, generated in Pt, and not from long-lived atoms: this hypothesis is statistically unlikely [30]. Because $\pi^+\pi^-$ atom generation in Pt cannot take place without Coulomb pair generation in the same material, the signal must originate from long-lived atoms.

In summary, the 2-dimensional analysis results in the following number of atomic pairs from $A_{2\pi}^L$ breakup in the Pt foil: $n_A^L = 436 \pm 61$. This corresponds to 7.1 standard deviations, taking into account statistical as well as systematic errors. In order to get an estimate for the expected number of atomic pairs, pion pairs generated in Be have also been analysed. To evaluate the initial value of Q_Y (Q_T), the momentum shift ΔQ_Y, due to the magnetic field, of 12.9 MeV/c has been subtracted from the reconstructed Q_Y. The 2-dimensional experimental $(|Q_L|, Q_T)$ distribution has been fitted by simulated distributions of atomic, Coulomb and non-Coulomb pairs from Be. Their corresponding numbers n_A, N_C and N_{nC} are free fit parameters. The total number of produced $\pi^+\pi^-$ atoms, $N_A = 17\,043 \pm 410$, has been obtained by using the precise (1%) ratio between N_A and N_C ($Q < Q_{cut}$), the number of detected Coulomb pairs with small Q [32]. Knowning from simulation (Section 4) that (4.0 ± 0.7)% of the produced atoms (N_A) break up in the Pt foil and the $(|Q_L|, Q_T)$ fit selection efficiency is 0.89, one estimates a generation of 607 ± 110 atomic pairs, and this does not contradict the measured number of 436 ± 61.

6. Conclusion

Long-lived $\pi^+\pi^-$ atoms have been observed for the first time in a dedicated experiment performed by means of the adapted DIRAC setup. Double-exotic $\pi^+\pi^-$ atoms are produced in ns states by 24 GeV/c CERN PS protons hitting a 103 μm thick Be target. The $\pi^+\pi^-$ pair analysis yields about 17 000 $\pi^+\pi^-$ atoms, based on the measured number of small Q Coulomb pairs. These atoms are moving in the target and interacting electromagnetically with Be atoms. About 7% of them leave the target in excited long-lived states. At a distance of 96 mm downstream of the Be target, a 2.1 μm thick breakup Pt foil has been installed. While passing through the gap between Be and Pt, some of the bound states (Table 1), mainly shorter lived states, are decaying, whereas the rest enters the Pt foil and about 90% break up, generating $\pi^+\pi^-$ atomic pairs:

$$n_A^L = 436 \pm 57|_{\mathrm{stat}} \pm 23|_{\mathrm{syst}} = 436 \pm 61|_{\mathrm{tot}}\,.$$

This result corresponds to a 7.1σ effect and does not contradict the estimated value of 607 ± 110. The observation of long-lived $\pi^+\pi^-$ bound states gives the possibility to study the *Lamb shift* and herewith a new $\pi\pi$ scattering length combination.

Acknowledgements

We are grateful to A. Vorozhtsov, D. Tommasini and their colleagues from TE-MSC/CERN for the Sm-Co magnet design and construction, R. Steerenberg and the CERN-PS crew for the delivery of a high quality proton beam and the permanent effort to improve the beam characteristics. The project DIRAC has been supported by CERN, the JINR administration, the Ministry of Education and Youth of the Czech Republic by project LG130131, the Istituto Nazionale di Fisica Nucleare and the University of Messina (Italy), the Grant-in-Aid for Scientific Research from the Japan Society for the Promotion of Science, the Ministry of Education and Research (Romania), the Ministry of Education and Science of the Russian Federation and Russian Foundation for Basic Research, the Dirección Xeral de Investigación, Desenvolvemento e Innovación, Xunta de Galicia (Spain) and the Swiss National Science Foundation.

References

[1] L. Nemenov, Yad. Fiz. 41 (1985) 980;
L. Nemenov, Sov. J. Nucl. Phys. 41 (1985) 629.
[2] B. Adeva, et al., Phys. Lett. B 704 (2011) 24.
[3] B. Adeva, et al., Phys. Lett. B 674 (2009) 11.
[4] B. Adeva, et al., Phys. Lett. B 735 (2014) 288.
[5] J. Uretsky, J. Palfrey, Phys. Rev. 121 (1961) 1798.
[6] S.M. Bilenky, et al., Yad. Phys. 10 (1969) 812;
S.M. Bilenky, et al., Sov. J. Nucl. Phys. 10 (1969) 469.
[7] H. Jallouli, H. Sazdjian, Phys. Rev. D 58 (1998) 014011;
H. Jallouli, H. Sazdjian, Phys. Rev. D 58 (1998) 099901 (Erratum).
[8] M.A. Ivanov, et al., Phys. Rev. D 58 (1998) 094024.
[9] J. Gasser, et al., Phys. Rev. D 64 (2001) 016008, arXiv:hep-ph/0103157.
[10] G.V. Efimov, M.A. Ivanov, V.E. Lyubovitskij, Yad. Fiz. 44 (1986) 460;
G.V. Efimov, M.A. Ivanov, V.E. Lyubovitskij, Sov. J. Nucl. Phys. 44 (1986) 296.
[11] A. Karimhodjaev, R.N. Faustov, Yad. Fiz. 29 (1979) 463;
A. Karimhodjaev, R.N. Faustov, Sov. J. Nucl. Phys. 29 (1979) 232.
[12] G.J.M. Austen, J.J. de Swart, Phys. Rev. Lett. 50 (1983) 2039.
[13] A. Gashi, et al., Nucl. Phys. A 628 (1998) 101.
[14] D. Eiras, J. Soto, Phys. Lett. B 491 (2000) 101.
[15] J. Schweizer, Phys. Lett. B 587 (2004) 33;
J. Schweizer, Eur. Phys. J. C 36 (2004) 483.
[16] G. Colangelo, J. Gasser, H. Leutwyler, Nucl. Phys. B 603 (2001) 125.
[17] J.R. Batley, et al., Eur. Phys. J. C 70 (2010) 635.
[18] J.R. Batley, et al., Eur. Phys. J. C 64 (2009) 589.
[19] L. Nemenov, V.D. Ovsyannikov, Phys. Lett. B 514 (2001) 247.
[20] L. Nemenov, V.D. Ovsiannikov, E.V. Chaplygin, Nucl. Phys. A 710 (2002) 303.
[21] B. Adeva, et al., CERN-SPSC-2011-001, cds.cern.ch/record/1319290.
[22] B. Adeva, et al., Updated DIRAC spectrometer at CERN PS for the investigation of $\pi\pi$ and πK atoms, Nucl. Instrum. Meth. (2015), submitted for publication.
[23] A. Vorozhtsov, et al., DN-2013-04 (DN=DIRAC-NOTE), cds.cern.ch/record/1622178.
[24] D. Dumitriu, DN-2014-02, cds.cern.ch/record/1755644.
[25] O. Gorchakov, DN-2014-03, cds.cern.ch/record/1755646.
[26] P. Batyuk, O. Gorchakov, V. Yazkov, DN-2012-03, cds.cern.ch/record/1475777.
[27] A. Benelli, V. Yazkov, DN-2013-03, cds.cern.ch/record/1622175.
[28] M.V. Zhabitsky, DN-2007-11, cds.cern.ch/record/1369651.
[29] V.D. Ovsiannikov, DN-2015-01, cds.cern.ch/record/2012229.
[30] V. Yazkov, DN-2015-02, cds.cern.ch/record/2012230.
[31] L. Afanasyev, et al., DN-2013-02, cds.cern.ch/record/1636206.
[32] L. Afanasyev, O. Voskresenskaya, Phys. Lett. B 453 (1999) 302.